Brown Algal Residue for the Recovery of Metal Ions-Application to La(III), Cd(II), and Ni(II) Sorption

Daniel Ballesteros-Plata, Yue Zhang, Enrique Rodríguez-Castellón, Vincent Thierry, Eric Guibal

Brown Algal Residue for the Recovery of Metal Ions—Application to La(III), Cd(II), and Ni(II) Sorption

Daniel Ballesteros-Plata, Yue Zhang, Enrique Rodríguez-Castellón, Thierry Vincent, and Eric Guibal**

Removing hazardous metals and recovering valuable strategic metals from wastewater has become an important challenge for the industry. Herein, brown algal biomass residue (AR, after bio-stimulant extraction, currently poorly valorized) is tested for the removal of Ni(II), Cd(II), and La(III) from aqueous solutions. This valorization of industrial waste makes profit of residual amounts of alginate-based materials, which have a strong affinity for metal cations. Fourier transform infrared (FTIR) and X-ray photoelectron spectroscopy (XPS) techniques are used for characterizing metal/biosorbent interactions. Uptake kinetics are relatively fast (equilibrium being reached in 180–240 min). The Sips equation fits the sorption isotherms; the maximum sorption capacities at pH ≈5 reach up to 0.84 mmol La g^{-1}, 0.92 mmol Cd g^{-1}, and 0.78 mmol Ni g^{-1}. In binary solutions, AR shows marked preference for La(III) over divalent cations. This selectivity may be increased by complexing base metals with EDTA, opening the route for the selective recovery of rare earth elements. HCl solution reveals more efficient (>90% for La(III), ≈82% for Cd(II) and Ni(II)) than $CaCl_2$ solution at pH 2 for metal desorption. This waste residue from biostimulant extraction (in brown algal biomass) can be valorized for the recovery of hazardous and strategic metal ions.

1. Introduction

Heavy and/or hazardous metals that are discharged into the environment, as industrial wastewater,[1] represent a major ecological and health problem given the toxicity of metals and their tendency to accumulate in the food chain.[2] Heavy and toxic metals are frequently found in the wastewater of many industries such as mining, foundry, electroplating (coating and protective treatments), surface finishing, battery manufacturing. Other strategic elements, such as rare earth elements (REEs)[3] (or noble metals[4]) are also discharged into the environment through industrial wastewater, also joining the food chain as they are not biodegradable. Increasingly strict legislation, together with the sustainability objectives proposed by the United Nations as well as proactive policies, make new waste recycling processes necessary to save resources and achieve sustainable development. Cadmium is mainly used in batteries (about 80% of production); another common use of this metal protective compound concerns electroplate steel (especially for aircrafts and oil platforms). Less developed application concerns the control of atomic fission in nuclear reactors (for neutron absorption).[5] Therefore, removing this metal from wastewater is of crucial importance. Along with Cd, other heavy metals such as Ni, Hg, Zn, Cu, Pb, or Cr are often found in wastewater;[1a] therefore, nickel may be another interesting tracer of metal contamination for developing alternative sorption processes. On the other hand, rare earths are extracted from their ores (after leaching step) by ion exchange and solvent extraction, which generates waste streams that are harmful to the environment.[6] Rare earths have also become strategic metals in high-tech industry; 90% of the world's extraction and production is mainly controlled by China.[7] The REE supply recently became a geostrategic and political issue worldwide for industries based on energy storage,[8] and electronic devices.[9] Cadmium and nickel are frequently associated with industrial waste (such as in rechargeable Ni-Cd batteries). On the other hand, LaNi alloys are used for hydrogen storage, they are also associated in metal hybrid batteries for hybrid cars.

There are many processes to recover or remove metals from wastewater streams, such as chemical precipitation, filtration membranes or ion exchange resins, among others.[1a,3a,10] However, most of these methods are generally expensive, they are not eco-friendly, they are inefficient especially at low metal concentrations,[11] and they can also generate new residues that, in turn, need to be treated.[12] Techniques such as bioremediation[13] or biosorption[14] can take advantage of the

D. Ballesteros-Plata, E. Rodríguez-Castellón
Department of Inorganic Chemistry
Crystallography and Mineralogy (Unidad Asociada al ICP-CSIC)
Faculty of Sciences
University of Málaga
Campus de Teatinos
Málaga 29071, Spain
E-mail: daniel.ballesteros@uma.es
D. Ballesteros-Plata, Y. Zhang, T. Vincent, E. Guibal
PCH
IMT – Mines Ales
Centre des Matériaux des Mines d'Alès
6 Avenue de Clavières, Alès Cedex F-30319, France
E-mail: eric.guibal@mines-ales.fr

reactive groups present in natural resources, biopolymers or agriculture residues.[11,15] In addition, these biosorbents are obtained as by-products of agriculture or industry; therefore, the cost of these alternative materials is significantly lower than those of synthetic resins and more sophisticated sorbents.[16]

Algae have the capacity to accumulate metal ions,[17] mainly due to the presence of several functional groups (hydroxyl, carboxylic, etc.) found on the surface of their cells,[18] and their abundance all over the world, their availability, low cost of preparation, their high adsorption efficiency, and retention capacity make these materials useful for metal recovery.[19] The sorption mechanism may involve the active transfer of metal ions across the cell membrane,[20] in addition to surface sorption on functional groups such as hydroxyl, carbonyl, amino, amide, phosphoryl, sulfhydryl groups.[21] In most cases, inactive algal cells exhibit higher sorption efficiency than living cells.[22] Brown algae have retained the attention of many researchers because of their high sorption capacity for metals, thanks to their high alginate content.[17b,21a,23] However, the use of algal biomass as a metal sorbent competes with other high added value applications such as the manufacture of biofuels,[24] or the extraction of active principles for cosmetic, biological and agricultural uses.[25] This fact, together with the increase in the price of algal biomass associated with physicochemical modifications, could question the competitiveness of the biosorption process.[26] Under these circumstances, and in line with the United Nation's Sustainable Development Goals, this work focuses on the valorization of a residue (after bio-stimulant extraction from *Laminaria digitata*), for the biosorption of metal ions. Combining the valorization of a residue with the recovery of valuable or hazardous metal ions contributes to these sustainable goals.[27] Romero et al. used a dealginated seaweed for cadmium biosorption;[18a] the dealgination of the material substantially decreased sorption properties (about 78%). Bulgariu and Bulgariu used an algal residue (after oil extraction from *Ulva lactuca* – green algae) for Cd(II) removal, achieving maximum adsorption capacities ≈0.20 mmol g^{-1} using raw algal residue,[28] and up to 0.31 mmol g^{-1} after alkaline treatment.[29]

This contribution focuses on the evaluation of the potential of the waste residue for the binding of base metal ions (considering here cadmium and nickel) and strategic rare earth element (lanthanum as an example). This purpose is reached after investigating the characterization of the material (and its interactions with metal ions), and extensively studying sorption performances. Separation properties are a key criterion for the design of sustainable processes for the recovery of strategic metals. In addition, a strategy is proposed (using EDTA as a selective ligand) for improving the separation of La(III) from Cd(II) and Ni(II). It should also be noted that AR has a minimal cost and does not require any pretreatment to be used as an adsorbent, which is a great advantage over other adsorbents, such as UiO-66 MOF,[30] or MXene based on $Ti_3C_2T_x$.[31] Indeed, these sophisticated inorganic metal/organic nanostructured sorbents require more complex synthesis and/or treatments that increase their cost and make difficult their large-scale application.[10a]

2. Results and Discussion

2.1. Characterization of Sorbent

2.1.1. SEM and SEM-EDX Analyses

Figure 1 shows the morphology of sorbent particles before and after the sorption of individual metal ions. A wide diversity of shapes can be observed: platelets, rounded particles with occasionally laminated structures (porous internal structure appears on broken pieces). The surface is irregular (superficial scaffold). Metal sorption does not change fundamentally the aspect and superficial texture of sorbent particles. Table S2, Supporting Information, reports the semi-quantitative EDX analysis of the surface of the sorbents (from Figure 1). The main changes appearing in these compositions logically concern the appearance of lanthanum, cadmium, and nickel in relevant samples. However, it is also important reporting the disappearance of some elements such as K, Na, Cl, and Mg, which are probably released during the sorption test as the results of wash-up or ion-exchange mechanism between target metal ions and these exchangeable cations. The case of calcium is a little different since after metal sorption the alkali-earths do not disappear: it is only slightly reduced for Ni(II) and Cd(II), and more significantly for La(III) Table S2, Supporting Information.

In Table S3, Supporting Information, the composition of the biomass (provided by the supplier, using proprietary analytical methods) is summarized: the presence of the alkali and alkali-earth elements is appearing as mineral fraction (about 20%). The extraction of the bio-stimulant hardly changes the alginate content in the biomass. Herein, alginate fraction reaches 32% (w/w); this is consistent with the order of magnitude usually cited for *L. digitata* biomass (between 20 and 52%, depending on the season etc.,[32]). The characterization of the alginate extracted from the residue shows that the mannuronic acid/guluronic acid ratio (M/G) ratio is close to 1; meaning that this alginate is useful for structuring soft and elastic gels.[32c] Other polysaccharides are also detected at trace levels, including laminarans (about 5%, w/w) and fucoidans. The presence of fucoidan (about 2%, w/w) corresponds to S content appearing in Table S4, Supporting Information (elemental analysis). Mannitol is also appearing at trace level (about 2%, w/w). Table S4, Supporting Information, also shows the presence of nitrogen, which may be associated to residual proteins. This overall composition means that the sorbent is mainly constituted of carboxylic acid groups (alginate-based material), and to much lower extent sulfonic groups (fucoidans), alcohol groups (mannitol), and amine groups (proteins).

2.1.2. FTIR Spectroscopy

To identify the functional groups (present in AR samples) that were involved in the interactions with metal ions (La(III), Ni(II) or Cd(II)), FTIR analyses are carried out on the samples collected from the tests on mono-component solutions. These spectra are compared to those of pristine AR and pre-treated sorbent at pH 5. The full spectrum is reported in Figure S1,

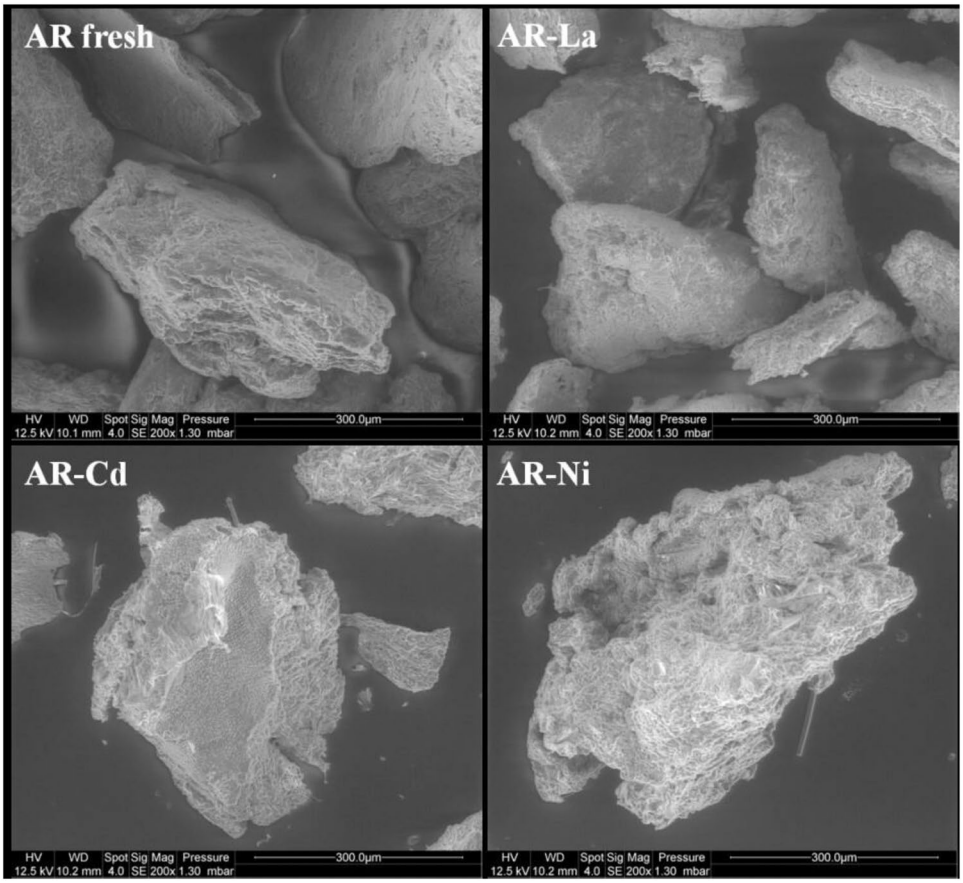

Figure 1. SEM images of AR fresh (particle size: 250–355 µm) and after La(III) (AR-La), Cd(II) (AR-Cd), or Ni(II) (AR-Ni) sorption.

Supporting Information, while **Figure 2** shows a focus on the 1800–500 cm^{-1} wavenumber range (where the most significant changes can be identified). The assignments and the relevant wavenumbers are summarized in Table S5 (Supporting Information). The broad band between 3340 and 3240 cm^{-1} is attributed to O—H and N—H stretching vibrations. The absorption peak that appears at 2920 cm^{-1} corresponds to the C—H vibrational modes in alkanes. Carboxylate groups can be identified by two bands at 1605 and 1408 cm^{-1} (asymmetric and symmetric stretching vibrations from COO^-, respectively). The important fraction of alginate in the residue may explain the presence of these strong bands. After metal sorption, these bands slightly shift toward lower wavenumbers, which suggests that these groups are involved in the binding of metal ions. Herein the $\Delta\nu(COO^-) = \nu_{as}(COO^-) - \nu_s(COO^-)$ is systematically lower than 200 cm^{-1}, highest values were obtained with raw and pH 5-treated biosorbent (197 and 189 cm^{-1}, respectively). After binding with divalent and trivalent cations, the value of $\Delta\nu(COO^-)$ decreases to 175 and 171 cm^{-1}, respectively. These values are consistent with those reported by Papageorgiou et al. in the analysis of direct interactions of alginate (carboxylic groups) with divalent metal cations (in the range 165–182 cm^{-1}: Cu(II)≈Zn(II) > Ca(II) > Ni(II) (174) > Cd(II) (168) > Pb(II)).[33] The value of $\Delta\nu(COO^-)$ may be correlated with the mode of interaction. They reported that when the $\Delta\nu(COO^-)$ value is higher than 200 cm^{-1} the preferential mode of interactions involves unidentate coordination. They finally established that the binding of divalent metal cations proceeds through the pseudo bridged unidentate bonding with polyguluronate moieties and through bidentate bridging coordination with polymannuronate. Herein, the M/G ratio being close to 1,

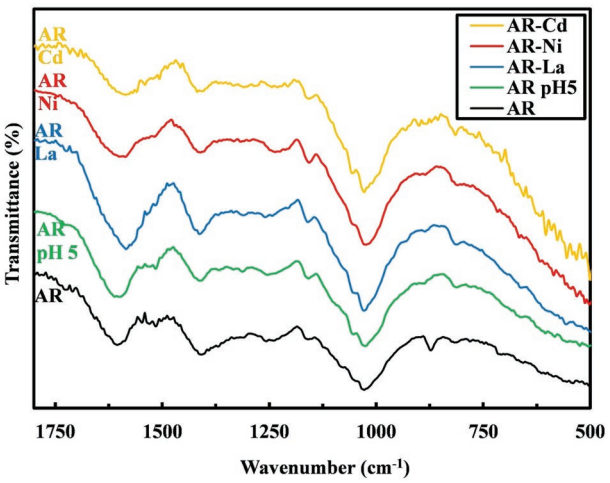

Figure 2. FTIR spectra for the sorbent (before and after contact with aqueous solution at pH_0 5) and after sorption of La(III), Cd(II), or Ni(II), at pH_0 5 (1800–500 cm^{-1} wavenumber range).

the sorbent is constituted of equivalent amounts of guluronate and mannuronate groups; $\Delta\nu(COO^-)$ remains below 180 cm^{-1}, meaning that the metal ions form bidentate coordinate with mannuronate units. The C—N—H groups (in protein and C(=O)-NHR moieties), which are identified at 1516 cm^{-1}, are poorly affected by the binding of metal ions. The amine groups are poorly represented (in terms of mass, Table S4, Supporting Information), the binding of metal ions to these groups would be in any case, difficult to detect. The pyranose ring is characterized by a series of bands at 1159 cm^{-1} (ν(C—O)) and 1078 cm^{-1} (assigned to ν(C—O) – (ν(C—C)).[34] After metal sorption, a shift of the band to 1028 cm^{-1} indicates that C—O functional groups are involved in the interactions with divalent and trivalent cations. The band at 874 cm^{-1} is shifted to ≈818 cm^{-1} after metal sorption (and after contact with pH 5 solution). The band at 874 cm^{-1} is generally assigned to carboxylic groups from β-mannuronic acid and α-L-guluronic acid. This shift may be associated with the ion-exchange mechanism responsible of metal binding onto carboxylic groups.[18a]

2.1.3. XPS Spectroscopy

XPS spectroscopy brings complementary information on the characterization of the sorbent and its interactions with metal ions. **Figure 3** reports the core level spectra of selected elements (with deconvolutions) for pristine sorbent (AR), the effect of conditioning at pH 5 (AR-5), and the spectra after metal sorption (AR-M, M = La, Cd, or Ni). Table S6, Supporting Information, reports the atomic concentration and weight percentage of major elements at the surface of the materials. These values differ from the elemental analysis reported in Table S4, Supporting Information; this is probably due to the heterogeneity of the material: XPS is a surface analysis while elemental analysis proceeds onto the whole mass of the sample. Table S7, Supporting Information, summarizes the information on the deconvolution of the core level spectra (including binding energies, BEs, and weight percentage). Figure 3a analyzes the core level of the C 1s signal for the different samples: at the surface of the sorbent C—OH, C=O, and O—C=O can be identified (correlated with the presence of alcohol, ketone, carbonate and carboxylate groups, consistently with FTIR analysis). Both the conditioning at pH 5 and the sorption of metal ions influence the shape of C 1s signal (meaning the respective contributions of the different functional groups). More specifically, the contributions of C—OH (major contribution: 18–26% atomic percentage) and C=O signals significantly increase with metal binding (especially for Cd and Ni uptake) (Table S7, Supporting Information). It is noteworthy that apparently in the case of Ni and Cd sorption, a new contribution appears (at the highest BE ≈289.2 eV, with a low atomic percentage: ≈2%) corresponding to carbonate species. In Figure 3b, the core level spectra of N 1s signal appear poorly affected by the conditioning of the sorbent and the interaction with metal ions; the weak proportion of nitrogen may also explain the difficulty to detect differences. Consistently with FTIR characterization, amine groups are not significantly contributing to metal binding. The data obtained for the O 1s spectrum (Figure 3c) show two main bands: one centered between 530.7–531.3 eV (hydroxyl groups) and another one centered between 532.4–532.8 eV, which is covering different types of functional groups: PO_4^{3-}, SO_4^{2-}, NO_3^-, ClO_3^- (covalent chloro), and C=O groups (identified at 531.97 eV for COOH-grafted SiO_2[35]). Figure 3d reports the specific bands of target metals (Ni 2p, Cd 3d, and La 3d). In the case of lanthanum, two peaks are identified at 835.2 and 838.2 eV, that correspond to the multiplet splitting of La $3d_{5/2}$ the binding energies and the ΔBEs both indicate that lanthanum is present as lanthanum oxide. Based on FTIR and XPS observations, it is possible concluding that La(III) is bound through interactions with alcohol, ketone, and carboxyl groups through oxygen atom.[36] For Cd $3d_{5/2}$ core level, a well-defined signal is observed at 405.4 eV (the Cd $3d_{3/2}$ signal is detected at 412.2 eV). This band corresponds to the interaction of Cd(II) with oxygen atoms.[37] In the spectrum of AR-Ni, the peak centered at 856.5 eV corresponds to Ni $2p_{3/2}$ signal, (associated with a satellite centered at 862.3 eV,[38]); the BEs for Ni $2p_{5/2}$ and its satellite are found at 873.8 and 879.6 eV, respectively. These peaks are assigned to Ni(II) species;[38] probably under the form of hydroxide, associated with oxygen atoms onto functional groups. Shao et al. also reported the shift on the peak associated with HO—C after lead removal, meaning that the hydroxyl oxygen atoms act as the binding sites for Pb(II) binding.[35]

Elemental analysis (semi-quantitative EDX determination), FTIR and XPS spectroscopies allowed to identify the major presence of carboxylate groups and their interactions with metal ions through ion-exchange of calcium with metal ions and complexation onto carboxylate groups.

2.2. Metal Sorption

2.2.1. pH Effect

The pH may influence both the speciation of the metal in the solution and the overall charge of the sorbent, which, in turn, play a major role in sorption mechanism and performances. **Figure 4** compares the effect of the pH on sorption capacity for the three metal ions. The profiles are very similar: the sorption capacity is negligible below pH 2.5. The pH being lower than the pH_{PZC} value (i.e., 3.7, see Figure S2, Supporting Information and detailed discussion), the protonation of the sorbent (main reactive groups being under the form of carboxylic acid) causes the repulsion of metal cations or hinders their binding. When pH increases, the repulsion effect progressively decreases, the carboxylate groups become favorable for metal binding and the sorption steeply increases. The percentage of carboxylic acid groups that are converted into carboxylate groups increases making possible the chelation of divalent and trivalent cations by carboxylate groups. The slope of the plot, in the range pH 2.5–4.5, decreases according the sequence: La(III) [0.77] > Cd(II) [0.60] > Ni(II) [0.59]. In terms of pK_a values, the metal ions can be ranked according to: La(III) [8.5] < Ni(II) [9.9] < Cd(II) [10.1]. It is not possible to correlate directly the impact of pH with the specific hydroxide formation constants. Above pH 4–5, the sorption capacity tends to stabilize. The sorption capacities are of the same order of magnitude for Cd(II) and Ni(II) (i.e., 0.64 and 0.69 mmol g^{-1}) and a little higher for La(III) (≈0.76 mmol La g^{-1}). The very close pH-edge profiles for the three metals indicate that the pH will not be an operative parameter for optimizing the separation of the metals while

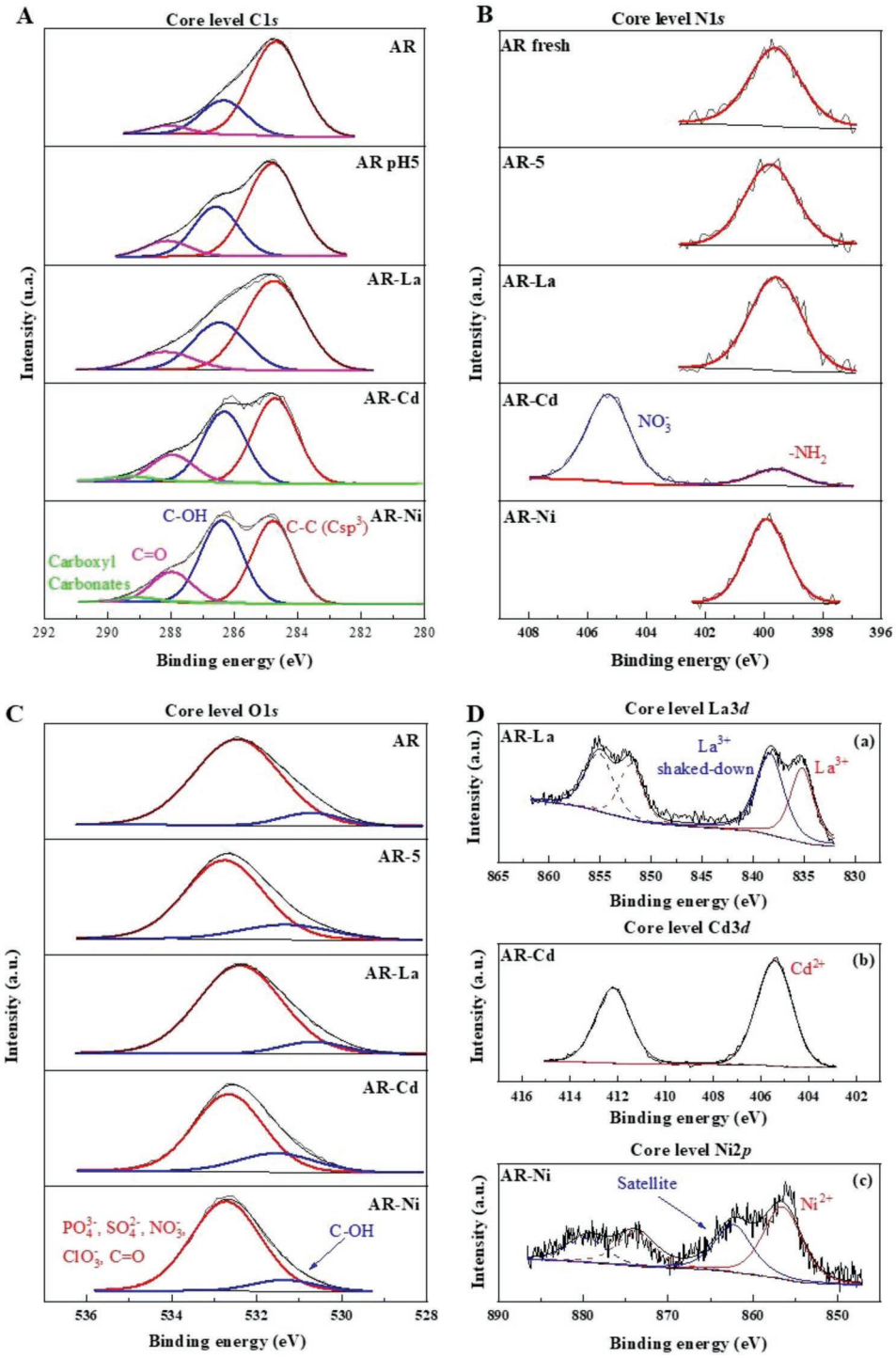

Figure 3. Core level spectra for pristine AR, after contact with pH 5 solution (AR-5) and La(III) (AR-La), Cd(II) (AR-Cd), or Ni(II) (AR-Ni) sorption for C 1s (A), N 1s (B), O 1s (C), and metal (D) (with a) La $3d_{5/2}$; b) Cd $3d_{5/2}$; and c) Ni 2p).

playing only on the pH. Figure S3a, Supporting Information, reports the pH variation occurring during metal sorption: the pH remains unchanged between pH 1 and 3. Above pH 3, the three metals show very different trends: in the case of Cd(II), the pH remains remarkably stable, while for Ni(II) the pH tends to increase (at least below 6). On the opposite hand, for La(III), the pH decreases slightly until pH 4 before dropping significantly (involving proton release or hydronium uptake). The behavior of divalent metal cations differs significantly from the trend followed by trivalent La(III). This means that the interactions of the sorbent with protons and metal ions involve different exchanges and stoichiometric ratios between divalent and trivalent cations. This is confirmed in Figure S3b, Supporting Information, the $\log_{10}$ plot of the distribution ratio D

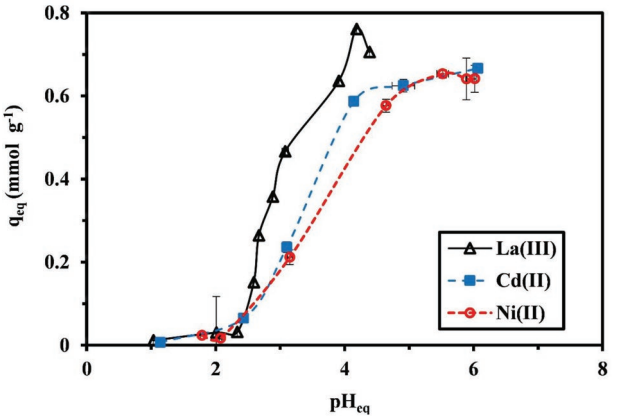

Figure 4. Effect of pH on metal sorption (Sorbent dose, SD: 0.5 g L^{-1}; C_0: 0.5 mmol L^{-1}; time: 48 h; T: 20 ± 1 °C).

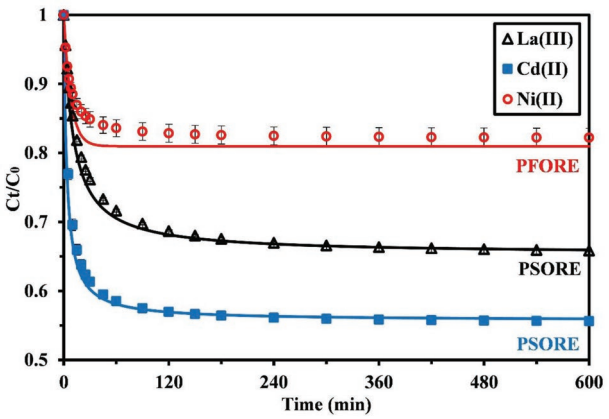

Figure 5. La(III), Cd(II), and NI(II) uptake kinetics – Modeling with the pseudo-first order rate equation (Ni(II) or the pseudo-second order rate equation (Cd(II) and La-(III)) (C_0: ≈1 mmol L^{-1}; pH_0: 5; SD: 0.5 g L^{-1}; *ν*: 180 rpm; T: 20 ± 1 °C).

(L g^{-1}) shows linear trends in the pH_{eq} 1–4 range with slopes decreasing from 0.77 (in the case of La(III)) to 0.58–0.60 (for Cd(II) and Ni(II)).

$$D = q_{eq} / C_{eq} \quad (1)$$

where q_{eq} and C_{eq} are the equilibrium sorption capacity and the residual metal concentration at equilibrium, respectively.

However, it is not possible to directly correlate the proton ion-exchange with the divalent and trivalent metal cations with the values of the slope (indicative of the stoichiometric proton exchange ratio in pure ion-exchange systems). Figure S4, Supporting Information, reports the speciation diagrams of La(III), Cd(II), and Ni(II) under the experimental conditions selected for the study of pH effect. The metal ions show significant differences: For La(III) and Ni(II) the metals are largely predominant (>90%) under their free form (La^{3+} and Ni^{2+}), regardless of the pH; on the opposite hand, cadmium is more sensitive to the pH due to the formation of chloro-species. Hence, above pH 3, more than 90% of the metal is present as free divalent species, while below pH 3, Cd^{2+} may coexist with cationic $CdCl^+$ (predominant below pH 2) and neutral $CdCl_2$ (less than 20% at pH 1). Despite these differences in the chemistry of metal species, the impact on the pH-edge profiles is relatively limited. All the species have comparable affinity with carboxylate groups in terms of pH response.

Based on these results and the possible occurrence of precipitation phenomena at pH > 6.5–7, further experiments were performed at pH_0 = 5. This is consistent with the majority of published work on lanthanum, cadmium, and nickel sorption (see below). The optimum pH corresponds to the deprotonation of the carboxylic acid, which enhances the binding of metal cations through chelation.

2.2.2. Uptake Kinetics

Uptake kinetics are mainly controlled by different mechanisms, associated with resistance to diffusion (bulk, film and intraparticle),[39] and the proper reaction rate (such as the pseudo-first and pseudo-second order rate equations).[40] Providing a sufficient agitation allows neglecting the effect of bulk diffusion and limiting the influence of resistance to film diffusion to the very first minutes of contact. **Figure 5** compares the uptake kinetics (under comparable conditions) for La(III), Cd(II) and Ni(II). The three curves show a very steep initial section: more than 50% of total sorption occurs within 10–15 min for La(III), 5 min for Cd(II), and 6 min for Ni(II). The $t_{90\%}$ (time for achieving 90% of total sorption) reaches 25–45 min for Cd(II), 15–25 min for Ni(II), and ≈105 min for La(III). The equilibrium is systematically achieved within 180 min. Based on these preliminary observations, the mass transfer properties follows the trend: Ni(II) > Cd(II) > La(III); mass transfer is favored by small ionic sizes (considering the ionic radius of hydrated metal species: Ni(II) [0.69 Å] < Cd(II) [0.95 Å] < La(III) [1.22 Å]).

The modeling of kinetic profiles (using the conventional equations reported in Table S1a, Supporting Information) is reported in **Table 1**. For La(III), the statistic parameters are very close for the three models (the RIDE, resistance to intraparticle diffusion equation, being slightly better); in the case of Cd(II), the best fit is obtained with the pseudo-second order rate equation (PSORE); while for Ni(II) the pseudo-first order rate equation (PFORE) gives better modeling. The calculated values of the sorption capacity at equilibrium ($q_{eq,1\ or\ 2}$, mmol g^{-1}) are consistent with experimental values ($q_{m,exp}$). The three metals obeying to different models, it is difficult to compare the rate coefficients; however, Table 1 clearly shows that all the kinetic rates (k_1 and k_2; i.e., the rate parameters for the pseudo-first and pseudo-second order rate equation, respectively) or the effective diffusion coefficient (D_e) for La(III) are lower than for the other divalent cations. The values of apparent rate coefficients (k_1 and k_2) are of the same order of magnitude than the values reported by Ammari Allahyari et al. for La(III) sorption onto metal–organic framework.[41] In the case of Ni(II) and Cd(II), Moreira et al. obtained higher values for k_1 and k_2 using another brown algae (*Fucus vesiculosus*).[42] The effective diffusion coefficients are D_e(La): 1.78 × 10^{-10} m^2 min^{-1}, D_e(Cd): 4.15 × 10^{-10} m^2 min^{-1}, and D_e(Ni): 4.63 × 10^{-10} m^2 min^{-1}. This is about two orders of magnitude lower than their self-diffusivity in water (i.e., D_0(La): 3.71 × 10^{-8} m^2 min^{-1},[43] D_0(Cd):

Table 1. Uptake kinetics for metal sorption using AR – Parameters of the models.

Model	Parameter	Unit	La(III)	Cd(II)	Ni(II)
Experimental	$q_{eq,exp.}$	mmol g^{-1}	0.643	0.750	0.433
PFORE	$q_{eq,1}$	mmol g^{-1}	0.629	0.716	0.410
	k_1	min^{-1}	0.0624	0.149	0.125
	R^2		0.943	0.966	0.977
	AIC		–163	–181	–248
PSORE	$q_{eq,2}$	mmol g^{-1}	0.666	0.739	0.423
	k_2	g $mmol^{-1}$ min^{-1}	0.143	0.395	0.524
	R^2		0.953	0.994	0.928
	AIC		–162	–221	–218
RIDE	De × 10^{10}	m^2 min^{-1}	1.78	4.15	4.63
	R^2		0.953	0.978	0.962
	AIC		–165	–180	–227

4.31×10^{-8} m^2 min^{-1} and D_0(Ni): 4.23×10^{-8} m^2 min^{-1},[44] respectively). In the case of La(III) removal using extractant impregnated resins, Kamio et al. reported diffusivity coefficient close to 4.5×10^{-10} m^2 min^{-1}.[45] Kolodynska et al. compared the pore diffusion coefficients for a series of ion-exchange resins:[46] the values ranged between 6.89×10^{-9} and 1.42×10^{-8} m^2 min^{-1}. While analyzing Cd(II) uptake kinetics onto calcium alginate beads, Papageorgiou et al. reported intraparticle diffusion coefficient close to 2.67×10^{-7} m^2 min^{-1}.[47] The resistance to intraparticle diffusion contributes to the overall control of uptake kinetics.

The three models fit well the experimental profiles (with varying preferences among the three metals); in any case, the resistance to intraparticle diffusion contributes to the control of kinetic profiles (in complement to the proper reaction rate).

2.2.3. Sorption Isotherms in Mono-Component Solutions

The equilibrium performances of the AR for the sorption of La(III), Cd(II), and Ni(II) at pH_0 5 are reported in **Figure 6**. While Cd(II) and La(III) sorption isotherms are very close (almost overlapped), the Ni(II) curve shows less favorable trend (lower saturation plateau, weaker initial slope). Based on these trends, the affinity of the sorbent (b_L coefficient in Langmuir equation, L $mmol^{-1}$) for these metals can be ranked according to: La(III) [236] > Cd(II) [30.6] > Ni(II) [6.04]. Considering the maximum sorption capacities (q_m, mmol g^{-1}), the metal ions can be ranked in a different order: Cd(II) [0.923] > La(III) [0.842] > Ni(II) [0.778]. The HSAB (hard and soft acid and base) theory assumes that hard acids preferentially react with hard bases (and reciprocally).[48] La (III) is considered a hard acid, contrary to Ni(II) (borderline class) and Cd(II) (soft acid); on the other hand, carboxylate groups are strong bases. The ranking in sorption parameters does not follow strictly the HSAB rules; the speciation of metal ions (formation of complexes) probably interferes with binding affinity.

The maximum sorption capacities for selected metals are compared with sorption performances of alternative biosorbents in **Table 2**. The AR shows sorption performances comparables to those of the most efficient algal systems (*Fucus spiralis*,[49]) for Cd(II) and Ni(II) removal; Vijayaraghavan et al. reports higher sorption of La(III) onto *Turbinaria conoides*.[50] Apart the comparison of AR with alternative biosorbents as appearing in Table 2, it is possible analyzing sorption performances against more sophisticated sorbents as reported in Table S8, Supporting Information. However, it is important pointing out that the advanced materials are generally significantly more expensive in terms of production costs, which, in turn may limit their application at large-scale. Another criterion to take into account concerns the life cycle of the sorbent. At the end of use, complex sorbents may require complex conditions of storage/inerting or thermal degradation, which are more expensive and/or more hazardous than for biosorbents such as AR.

Table 3 summarizes the parameters of the models used for fitting sorption isotherms. The Sips equation, which consists of a combination of Langmuir and Freundlich equations (Table S1b, Supporting Information), shows the highest statistical criteria. The Langmuir equation supposes a monolayer sorption of target solute, without interaction between sorbed

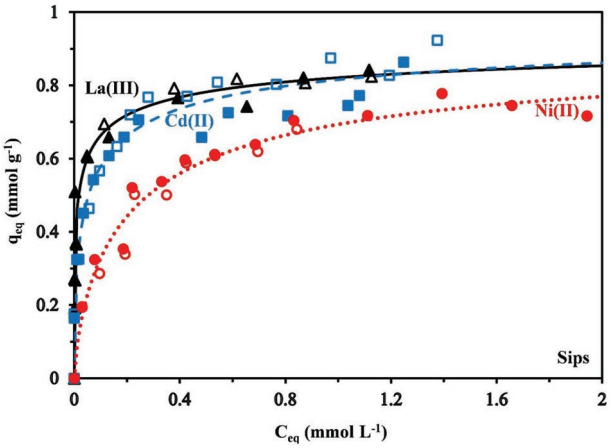

Figure 6. La(III), Cd(II), and Ni(II) sorption isotherms at pH_0 5 – Modeling with the Sips equation (SD: 0.5 g L^{-1}; T: 20 ± 1 °C; time: 48 h; *v*: 180 rpm).

Table 2. Comparison of Ni(II), Cd(II), and La(III) sorption capacities for a series of biosorbents.

Metal	Biosorbent	C_0 [mmol L^{-1}]	Particle size [mm]	SD [g L^{-1}]	pH	q_m [mmol g^{-1}]	Ref.
Ni(II)	AR	1	0.25–0.35	0.5	5	0.777	[a]
	Cystoseira indica	0.5	0.5–1.0	2	6	0.181	[12]
	Cystoseira indica	0.1	–	0.8	5	0.172	[21a]
	Fucus spiralis	0.85	<0.5	0.5	6	0.852	[49]
	Ascophyllum nodosum	0.85	<0.5	0.5	6	0.738	[49]
	Durvillaea antartica	5	0.5–1	–	5	0.599	[51]
	Ulva lactuca	4.2	–	0.5	5	0.652	[52]
Cd(II)	AR	1	0.25–0.35	0.5	5	0.923	[a]
	Cystoseira indica	0.5	0.5–1.0	2	5.5	0.173	[12]
	Chlorella vulgaris	0.89	0.25–0.3	1	4.5	0.831	[53]
	Dealginated seaweed waste	1.5	–	1	6	0.670	[18a]
	Chemically-treated *Saccharomyces carpophyllum*	0.1	–	0.8	5	0.761	[21a]
	Raw green algal waste	0.4	–	8	5	0.300	[29]
	Coelastrelal sp.	0.02	0.01	–	5.5	0.578	[54]
	Fucus spiralis	0.44	<0.5	0.5	6	1.022	[49]
La(III)	AR	1	0.25–0.35	0.5	5	0.842	[a]
	Turbinaria conoides	0.72	0.75	–	4.9	1.11	[50]
	Sargassum fluitans	5	3–5	2.5	5	0.730	[55]
	Chlorella vulgaris	1.08	–	0.53	6	0.539	[56]
	Chlamydomonas reinhardtii	1.08	–	0.53	6	1.03	[56]
	Pseudomonas sp.	0.72	–	0.5	5	0.864	[57]

[a] This study (AR).

molecules, and the sorption energy being homogeneous at the surface of the sorbent. The Freundlich equation (fundamentally empirical) is correlated with possible interactions between bound solutes; this type of equation is frequently appropriate when the concentration range is not wide enough to make possible the saturation of the sorbent. Herein, the third adjustable parameter of the Sips equation allows improving the quality of the fit, at the expense of a loss in the phenomenological interpretation of sorption mechanism. Actually, the calculated values of the saturation capacity overestimate the experimental sorption capacities. Consistently with previous observation on b_L, the $b_s^{n_s}$ (affinity coefficient in Sips equation elevated to its Sips exponent) values follow the sequence: La(III) [66.8 L $mmol^{-1}$] > Cd(II) [19.3] > Ni(II) [4.55]. Apparently, the sorbent has a greater affinity for La(III) against divalent metal cations. This conclusion needs confirmation through the study of sorption performance from multi-component solutions (see Section 4.2.4.). Table S9, Supporting Information, reports the main physicochemical properties of selected metals. The affinity of AR (b_L and $b_s^{n_s}$ values) varies as the reciprocal of the Pauling electronegativity (X_m) and increases with ionic radius of hydrated species (r_P). Figure S5, Supporting Information, shows the mapping of selected elements in the frame formed by ionic radius Z^2/r_p and covalent index ($X_m^2 \times r_p$), the bubble size is correlated to the $b_s^{n_s}$ values. Cd(II) and Ni(II) are ranked in the intermediate class while La(III) is part of Class A (hard metals). Sorption isotherms are best fitted using the Sips equation and the maximum sorption capacities for the three metals range between 0.78 and 0.92 mmol g^{-1}. The differences are more significant in terms of affinity coefficient (La>>Cd>>Ni).

2.2.4. Sorption Selectivity in Bi-Component Solutions

The selectivity property of the sorbent is a key criterion for the design of sustainable processes for the recovery of strategic metals (and more globally the valorization of removed metal ions). In this section, the sorption of La(III) and Ni(II) from binary solutions (at pH_0 5) is illustrated in **Figure 7**a for different molar ratios between the two components, while Figure 7b compares the sorption of La(III) and Cd(II) from binary solutions. The results show that the sorption of La(III) in the presence of Ni(II) is weakly decreased, even in excess of Ni(II): the saturation capacity decreases from 0.77 ± 0.03 (La:Ni = 3:1) to 0.69 ± 0.07 (La:Ni = 1:1), and 0.65 ± 0.04 mmol La g^{-1} (La:Ni = 1:3); compared with 0.84 mmol La g^{-1} in monocomponent solution. On the opposite hand, the presence of lanthanum strongly decreases nickel binding: the maximum sorption capacity

Table 3. La(III), Cd(II), and Ni(II) sorption isotherms – Parameters of the models.

Model	Parameter	Unit	La(III)	Cd(II)	Ni(II)
Experimental	$q_{m,exp.}$	mmol g^{-1}	0.842	0.923	0.778
Langmuir	$q_{m,L.}$	mmol g^{-1}	0.765	0.817	0.812
	b_L	L $mmol^{-1}$	236.5	30.55	6.040
	R^2		0.874	0.932	0.960
	AIC		–96	–137	–167
Freundlich	k_F	$mmol^{1-1/n_F}$ L^{1/n_F} g^{-1}	0.854	0.830	0.677
	n_F		6.64	5.84	3.66
	R^2		0.905	0.928	0.933
	AIC		–103	–139	–154
Sips	$q_{m,S.}$	mmol g^{-1}	0.971	0.989	0.919
	b_S	$(L\ mmol^{-1})^{1/n_S}$	5.48	4.71	3.07
	n_S		2.47	1.91	1.35
	R^2		0.925	0.944	0.966
	AIC		–105	–141	–170

$q_{m,exp}$ is the maximum sorption capacity (experimental value), $q_{m,L}$ and $q_{m,S}$ are the maximum sorption capacities for Langmuir and Sips equations, respectively (calculated values); b_L and b_S are the affinity coefficients for Langmuir and Sips equations, respectively; n_F and n_S are the exponential parameters of the Freundlich and Sips equation (related to sorption intensity), respectively; k_F is the constant related to sorption capacity according Freundlich equation.

does not exceed 0.06 mmol Ni g^{-1} (against 0.78 mmol Ni g^{-1} in mono-component solution) when La(III) is in excess (i.e., La:Ni = 3:1). When the relative concentration of Ni(II) increases the sorption capacity of Ni(II) slightly increases up to maximum values close to 0.16–0.28 mmol Ni g^{-1}; meaning far below than the maximum sorption capacity in mono-component solution. It is noteworthy that for La:Ni ratio 1:1 and 1:3, nickel sorption isotherms show an unexpected trend: a maximum in sorption capacity is reached for residual Ni concentrations close to 0.1 and 0.15–0.25 mmol Ni L^{-1}, before slightly decreasing. Ni(II) and La(III) are competing for the same reactive groups (cumulative sorption capacity varies between 0.75 and 0.85 mmol g^{-1}). The higher affinity of La(III) inhibits nickel uptake (**Figure 8**b). On the opposite hand, the higher affinity of Cd(II) for the sorbent (compared with Ni(II)) induces stronger effect on La(III) sorption, especially in the case of cadmium excess (maximum sorption capacity decreases to 0.61 ± 0.03 mmol La g^{-1}). The most significant difference is observed for Cd maximum sorption capacity that decreases less than for Ni(II): the maximum sorption capacities are found close to 0.22 mmol Cd g^{-1} (La:Cd = 1:1) and 0.32 mmol Cd g^{-1} (La:Cd = 1:3). Compared with Cd(II) maximum sorption capacity in mono-component solutions (i.e., 0.92 mmol g^{-1}), the loss in sorption capacity in the presence of La(III) is of the same order than for Ni(II). Overall, the AR shows outstanding selectivity for La(III) over Ni(II) and Cd(II) in competitive sorption. Notably, da Costa's group confirmed that the removal efficiency of REE(III) (yttrium) was not significantly influenced by the presence of competitive cations, Co(II).[58] Wu et al. also found that the La(III) removal efficiency of magnetic Ca-alginate beads was not significantly influenced by the co-existence of divalent cations (e.g., Pb(II), Cd(II), Co(II), Ni(II)).[59] These reports are consistent with the higher binding affinity of carboxylic groups in alginate backbone for trivalent cations (e.g., REE^{3+}) compared with divalent cations.[60]

The competitive Sips equation was used to fit the 3D sorption isotherms for La/Ni (Figure 8a) and La/Cd (Figure 8b) bi-component systems.

$$q_{Mi,eq} = \frac{q_M \times b_{S,Mi} \times C_{eq,Mi}}{1 + \left(b_{S,Mi} \times C_{eq,Mi}^{\frac{1}{n_{S,Mi}}}\right) + \left(b_{S,Mj} \times C_{eq,Mj}^{\frac{1}{n_{S,Mj}}}\right)}, i \neq j \quad (2)$$

With q_M, total sorption capacity (mmol g^{-1}); b_s, Sips affinity coefficients (mmol L^{-1})n_S; n_s, exponential Sips coefficient (dimensionless).

The plots fit well experimental profiles; the generated surfaces confirm the weak competition of Ni(II) and Cd(II) onto La(III) sorption, while the presence of La(III) drastically reduces the binding of divalent cations. Indeed, La(III) is characterized by a convex–type surface, contrary to the concave surfaces for Cd(II) and Ni(II). This is confirmed by the values of the affinity coefficients reported in Table S10, Supporting Information: the affinity coefficients for La(III) are about one order of magnitude higher than the corresponding affinity coefficient for competitor divalent cation.

The selectivity of the sorbent for lanthanum against competitor metal ions ($SC_{La/metal}$, dimensionless) is defined as the ratio of distribution coefficients (D_{La}/D_{metal}), and:

$$SC_{La/metal} = \frac{D(La)}{D(metal)} = \frac{q_{eq}(La) \times C_{eq}(metal)}{C_{eq}(La) \times q_{eq}(metal)} \quad (3)$$

The $SC_{La/Ni}$ values are remarkably high in the weak concentration ranges (i.e., below 0.2, especially when lanthanum is not in excess in the solution) with values that may reach up to 200–660. When lanthanum is in excess, the SC values strongly reduce; however, even under these less favorable conditions, the

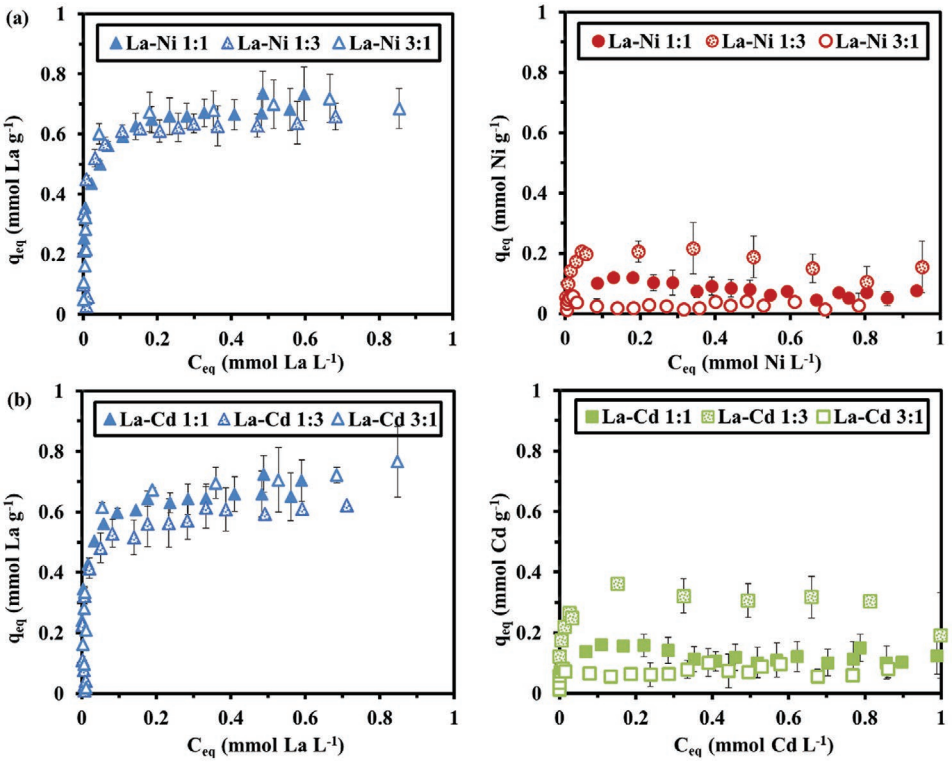

Figure 7. Sorption isotherms of a) La(III)-Ni(II) and b) La(III)-Cd(II) from bi-component solutions at pH_0 5 – with variable molar ratio of metal concentrations: 1/1, 1/3, and 3/1 (SD: 0.5 g L^{-1}; T: 20 ± 1 °C; time: 48 h; *ν*: 180 rpm).

lowest values of $SC_{La/Ni}$ exceed 10. Basically, the same trends are observed for the competition between La(III) and Cd(II); however, the values of the SC parameter are systematically lower than those reported for Ni(II), due to the higher affinity of AR for Cd(II), which is exerting a stronger competitive effect on lanthanum binding. Figure S7, Supporting Information, shows the plots of $SC_{La/metal}$ as a function of the molar ratio La/metal for Ni(II) (Figure S7b, Supporting Information) and Cd(II) (Figure S7b, Supporting Information). This figure confirms and summarize the conditions that enhance the selectivity of the sorbent for lanthanum: $SC_{La/metal}$ strongly decreases with the molar ratio of residual concentrations La/Metal, following a negative power function: the negative power coefficient is logically higher for Cd(II) (i.e., –0.73) than for Ni(II) (i.e., –0.60). The higher affinity of the sorbent for La(III) against Cd(II) and Ni(II) is consistent with the gradient in affinity coefficient (as reported in Section 2.2.3.). While the presence of La(III) drastically reduces the uptake of divalent cation, the presence of cadmium and nickel hardly affects the lanthanum uptake.

2.2.5. Selectivity Enhancement by Metal Speciation Modulation

The strategies for improving sorption performance or sorption selectivity may consist in incorporating specific functional groups with tailored structure arrangement through different methods, such as ion-imprinting,[61] or oriented hydrogel formation.[62] However, the selective separation of rare earths may be also enhanced with controlled complexation.[63] This concept was frequently used in liquid/liquid extraction of rare earths: playing with different soluble ligands such as EDTA, DTPA (diethylenetriaminepentaacetic acid), or HEDTA (diethylenetriaminepentaacetic acid), allowed separating yttrium from heavy lanthanides.[64] The comparison of the formation constants for ligand/metal allows anticipating on the enhancement of the selective separation: the greater the difference in the pK_f values for the competitive metals ions, the easier the separation of the metals. Table S11, Supporting Information, reports the formation constants of different metals with EDTA, including La(III), Ni(II), and Cd(II).

Figure 9 shows the fraction of sorbed metals on AR for La(III)/Ni(II) (Figure 9a) and La(III)/Cd(II) (Figure 9b) systems in absence and presence of EDTA. Clearly, in the case of Ni(II) competition, the introduction of EDTA increases the relative fraction of La(III) in AR (systematically higher than 94%, Figure S9, Supporting Information); in addition, the effect of metal concentration has a weaker impact on this distribution compared with the test without EDTA. These effects are less marked in the case of the La/Cd system; though the presence of EDTA improves the accumulation of La(III) in the sorbent. In the case of Ni(II) competition (as shown in Figure S8b, Supporting Information), the addition of EDTA increases both the affinity of the sorbent (steepest initial slope) and the maximum sorption capacity for La(III) (from ≈0.6 mmol to ≈0.7 mmol La g^{-1}). This enhancement of lanthanum sorption may be explained by the preferential complexation of Ni(II) that becomes less adsorbable and less competitor; therefore, a greater number of reactive groups remains available for La(III) binding. Figure S7, Supporting Information, shows the speciation diagrams for La/Ni/EDTA system and La/Cd/EDTA

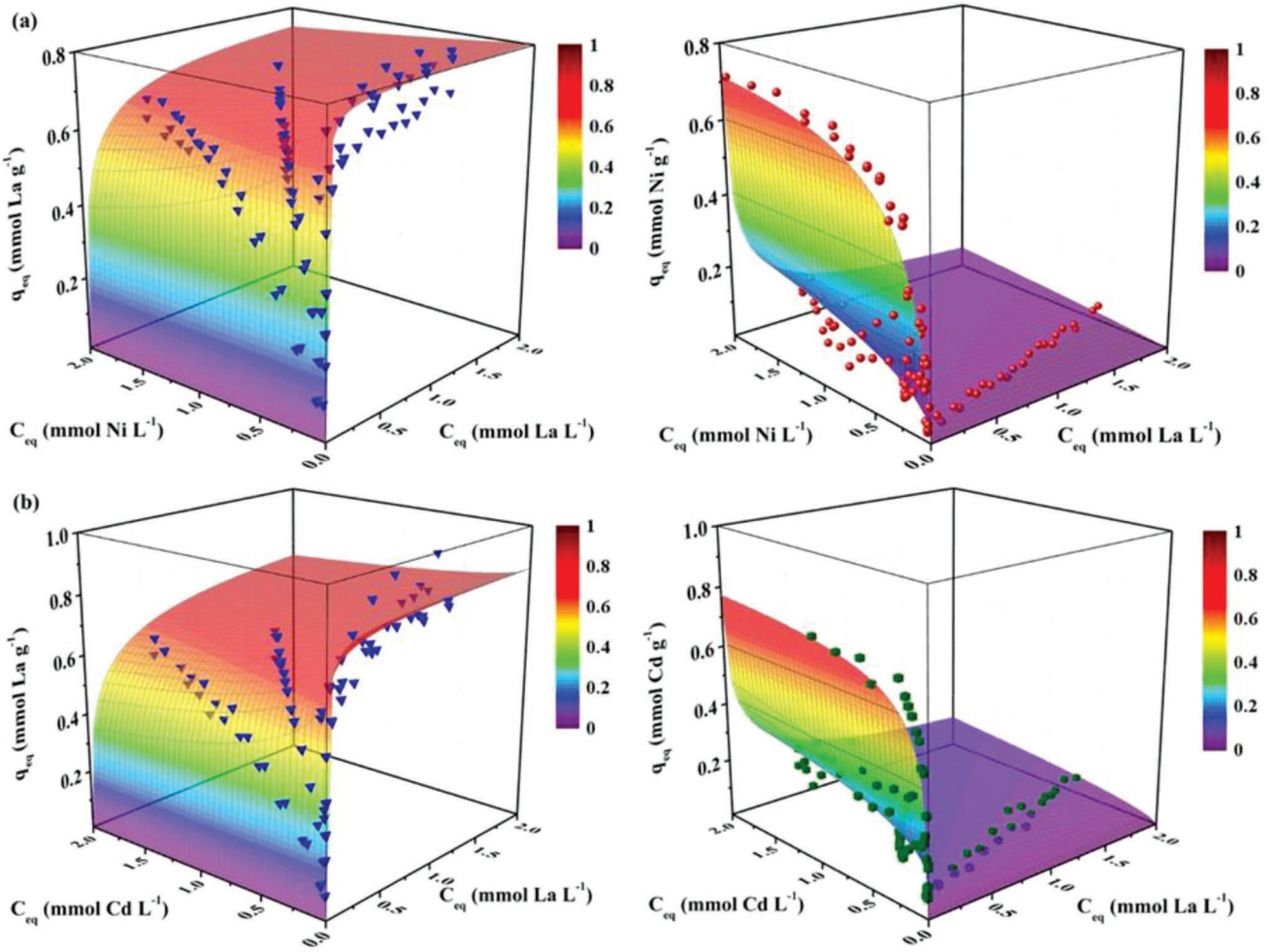

Figure 8. 3D plots of sorption capacities against residual metal concentrations (a) La-Ni, b) La-Cd – Surfaces generated by the competitive Sips equation.

system (equimolar concentrations for each component at pH_0 5). In the case of La(III)/Ni(II) (Figure 7a), La(III) is present as free species (≈97%), which are readily adsorbable onto AR sorbent; on the opposite hand, free nickel represents less than 8%. Ni(II) mainly present as $NiEDTA^{2-}$ (about 95%) is poorly adsorbable (anionic repulsion with carboxylate groups). Metal speciation confirms the hypothesis of decreased competition effect of Ni(II) against La(III), which, in turn, improves La(III) sorption. A distinct pattern can be observed in the case of La(III)/Cd(II) system (Figure 7b). Indeed, the introduction of EDTA decreases the sorption capacity and affinity coefficient (initial slope) for both La(III) and Cd(II). Figure S7b, Supporting Information, reports the speciation of La(III) and Cd(II): free lanthanum only represents ≈60% while free Cd(II) counts for ≈40% of total cadmium; the remaining fractions are formed of relevant EDTA complexes that have lower affinity for AR. Therefore, the sorption capacities decrease because of lower availability of free adsorbable species. The weaker effect of EDTA on the separation of La/Cd (compared with La/Ni) can be explained by the respective values of $\Delta \log K_f$ that reaches 3 units in the case of La/Ni and only 1.1 for La/Cd (Table S10, Supporting Information).

The selectivity coefficients are compared in Figure S10, Supporting Information, for two configurations (without and with EDTA). For Cd(II) competition, the introduction of EDTA slightly improves the selectivity coefficient (which can reach up to 40), especially at low metal concentrations (i.e., ≈0.2–0.3 mmol L^{-1}). However, this enhancement is negligible compared with the case of Ni(II) competition, where the $SC_{La/Ni}$ values may reach several thousands (and up to tens of thousands at C_0: 0.25 mmol L^{-1}). These behaviors may be correlated to the speciation discussion: the formation of Ni-EDTA complexes limits the availability of free Ni(II) species for binding on reactive groups (which can readily bind free predominant free lanthanum species). The preferential complexation of Ni(II) with EDTA (compared with Cd(II) and even more so with La(III)) allows improving the selective sorption of lanthanum from competitive divalent cations.

2.2.6. Metal Desorption and Sorbent Recycling

The recovery of metals from loaded sorbents and the recyclability of the sorbents are key parameters in the design of new

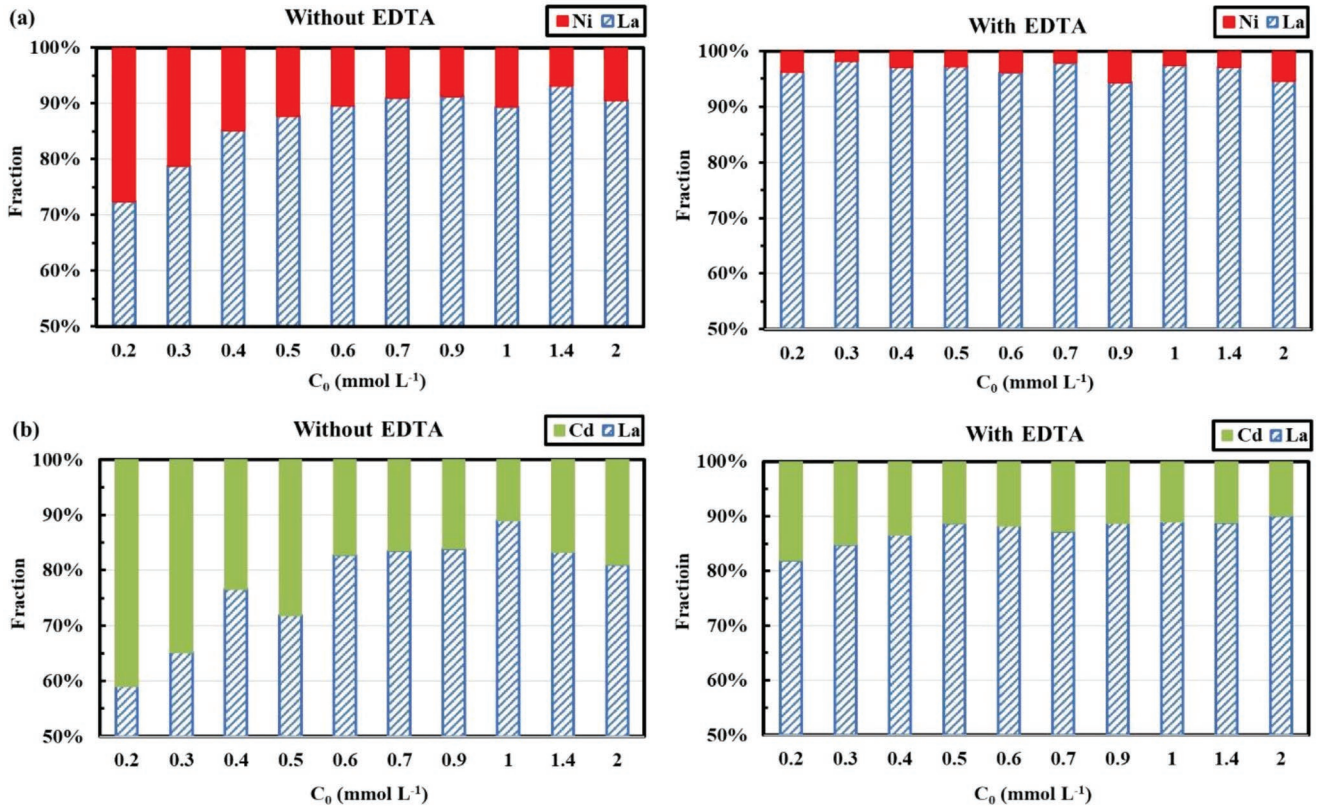

Figure 9. Fraction of sorbed metals (a) La(III)-Ni(II), and b) La(III)-Cd(II)) from bi-component solutions at pH_0 5, in absence and presence of EDTA at equimolar concentrations (SD: 0.5 g L^{-1}; T: 20 ± 1 °C; time: 48 h; *ν*: 180 rpm).

sorbents. **Figure 10** compares the sorption capacity and desorption efficiency for five successive cycles with two types of eluents: HCl solution and 0.05 M $CaCl_2$ solutions (both at pH 2). Based on the study of the pH effect on the sorption of metal ions, acidic solutions are capable of reversing the binding of target metal ions. The pH was selected with the objective of limiting the degradation of the biosorbent. The use of $CaCl_2$ was driven by a dual target: a) the possibility to use Ca^{2+} ions as a cation exchanger, and b) the stabilization of alginate fraction by ionotropic gelation of carboxylate groups with Ca^{2+}. In Figure 10, the best elution and best recyclability are obtained with HCl solution. At the first cycle, the desorption of La(III) reaches 96% (86% and 85% for Cd(II) and Ni(II), respectively); much higher than with 0.05 $CaCl_2$-pH 2 solution (94% for La(III) and 65%–67% for divalent metal cations). With recycling the sorbent, the efficiency in desorption progressively decreases, especially for Ni(II) (only 62% at the fifth cycle), while for the other metals the loss in desorption efficiency remains at 82% for Cd(II) and up to 91% for La(III) with HCl eluent. The losses in desorption are significantly greater with $CaCl_2$ solutions. The incomplete desorption may explain the progressive decreases in sorption capacities, which reach, in the case of HCl eluent, at the fifth cycle: 39%, 48%, and 62% for La(III), Cd(II), and Ni(II) respectively. For $CaCl_2$ eluent, the decreases reach 41%, 45%, and 60%. There are other reasons complementary to the incomplete desorption for explain the loss in sorption performances, including the probable degradation of the sorbent. It is noteworthy that despite the loss in sorption performance, the sorption capacities maintain ≈0.4 mmol g^{-1} for La(III) and Cd(II) at the fifth cycle. Considering that the AR is a waste, which is used without chemical modification, the sorption performance remains attractive. Much higher stability in sorption property was obtained with alternative functionalized sorbents;[65] however, these sorbents are considerably more complex and expensive (in these cases, the long-term stability recycling is required). HCl solution (at pH 2) succeeds in recovering metal ions (in the range of 70–95%) for the first four cycles of reuse (larger decrease at the fifth cycle); therefore, the sorption capacity decreases progressively (marked effect decreases according to: Ni(II) > Cd(II) > La(III)).

3. Conclusions

The valorization of AR (issued from the extraction of agriculture bio-stimulants from *L. digitata*) without complementary treatment is successfully tested for the sorption of a REE (lanthanum) and two divalent cations (Ni(II) and Cd(II)). Sorption performances are comparable to those reported for conventional algal sorbents. The sorption mainly occurs onto carboxylic groups present on the AR (as confirmed by FTIR and XPS analysis) at the optimum pH (i.e., pH 5).

Under selected experimental conditions, the equilibrium of kinetics is reached within 180–240 min; the kinetics can be fitted by PFORE (for Ni(II)) and PSORE (for Cd(II) and La(III)). The sorption isotherms are successfully modeled using the Sips

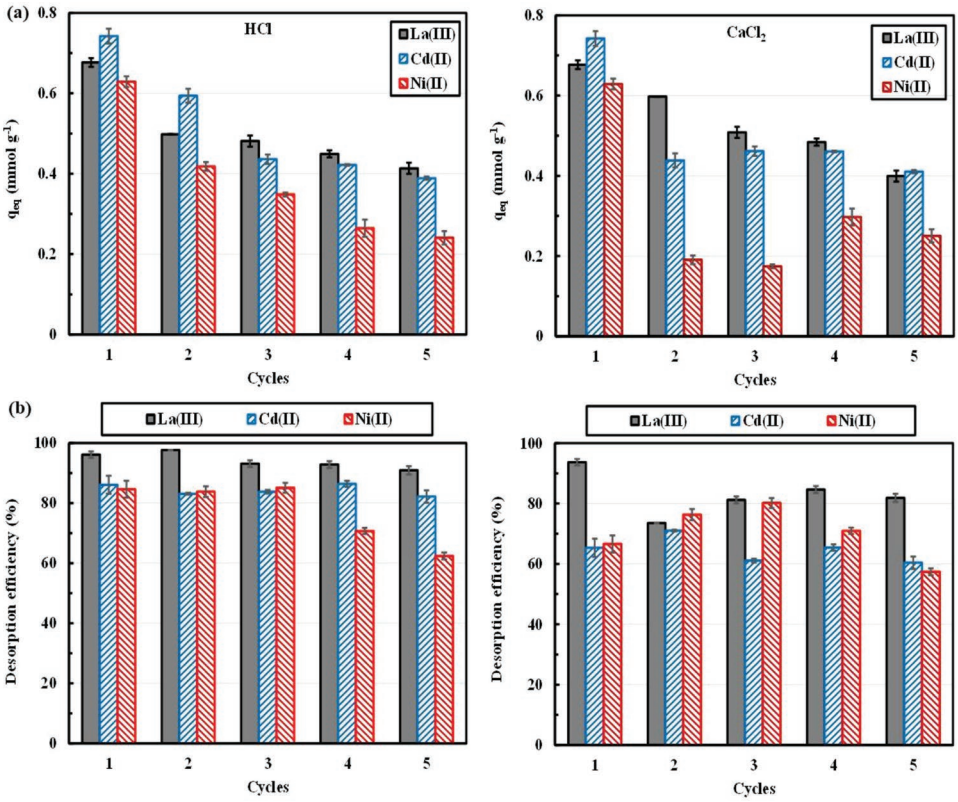

Figure 10. Sorbent recycling – a) Sorption capacity and b) desorption efficiency for 5 successive cycles (mono-component solutions, SD: 0.5 g L^{-1}; T: 20 ± 1 °C; time: 48 h (sorption test) and 24 h (desorption test); *v*: 180 rpm; eluents: $CaCl_2$ and HCl solutions at pH 2).

equation and the maximum sorption capacity reaches levels comparable to the values reported for usual brown algae. This may be explained by the relatively high proportion of alginate in the AR. The affinity of the sorbent for selected metals ions shows a marked preference for La(III) against selected divalent cations. The ranking in affinity (La(III) > Cd(II) > Ni(II)) is correlated with the ionic size of hydrated species and inversely correlated with the Pauling electronegativity. In bi-component solutions the sorbent has marked preference for interacting with La(III) especially against Ni(II). The metal speciation may be tuned with soluble ligand (such as EDTA) to enhance metal separation. This is effective in the case of La separation from Ni because of the large difference in the EDTA-metal formation constant (between La(III) and Ni(II)). This effect is more limited for La(III) separation from Cd(II) (closer values of formation constants) and formation of less adsorbable species (EDTA-La and EDTA-Cd complexes). EDTA can be used for improving the separation between La(III) and Ni(II), not for selectively recovering La(III) from Cd(II) solutions.

Obviously, for evaluating the real potential of this sorbent it would be necessary to test the sorption properties from complex industrial solutions. Another issue would consist in designing the operating system for its practical application. Using small size particles (as the current study) may cause problems in terms of solid/liquid separation in agitated reactor or hydrodynamic problems in fixed bed systems (typical for resin-type sorbents) such as heal loss pressure and/or flow blockage. Granulating the sorbent would help in solving these problems, pending optimization for minimizing loss in mass transfer properties and/or availability of reactive groups.

4. Materials and Methods

Materials: The AR was obtained after the extraction of agriculture bio-stimulants from the brown algae *L. digitata* by Algaia SA company (Lannilis, France). The AR was sieved into different particle sizes, in the range 63–1000 µm. After a preliminary study with each particle size, it was decided to use the AR sample with an intermediate particle size, between 250 and 355 µm (compromise between easier solid/liquid separation and kinetic observations). AR had been used for investigating sorption properties without any physical or chemical treatment prior to sorption tests.

Lanthanum ($LaCl_3 \cdot xH_2O$), cadmium ($CdCl_2 \cdot H_2O$) were provided by Merck AG (Darmstadt, Germany) and nickel ($NiCl_2$ anhydrous) was purchased from Riedel-de Haën (Honeywell, Charlotte, NC, USA). HCl and NaOH were used for the pH adjustment. All solutions were made with deionized water. Calcium chloride ($CaCl_2 \cdot 2H_2O$ (>99.5%) was purchased from Chem-Lab (Chem-Lab NV, Zedelgem, Belgium). Ethylenediaminetetracetic acid (EDTA, $[CH_2N(CH_2COOH)_2]_2$, purity 99%) was supplied by AnalytiCals (Milan, Italy). All chemicals used were of analytical grade.

Characterization of Sorbent: For the analysis of the functional groups present in the samples, before and after sorption, FTIR

analysis was performed in the range 4000–400 cm^{-1} using a Bruker VERTEX 70 spectrometer (Bruker, Germany) equipped with an ATR (attenuated total reflectance tool). The morphology and the composition of the samples, pristine and after metal sorption, were analyzed using a scanning electron microscope (SEM, FEI Quanta 200F) equipped with an Energy Dispersive X-ray accessory (EDX). XPS spectra were collected on a Physical Electronics PHI 5701 spectrometer in order to determine the superficial composition. A non-monochromatic Mg-Kα radiation (720 µm, 300 W, 15 kV, 1253.6 eV) and a multi-channel detector had been employed. Samples had been analyzed in a constant pass energy mode at 29.35 eV. Charge referencing had been calibrated against C 1*s* at 284.8 eV of adventitious carbon. Elemental chemical analysis (CHN) was used to determine the C, H, N, and S percentage in the fresh samples with different particle sizes (from 63 to 1000 µm); analyses were carried out using an EuroA3000 CNHS-O analyzer (Eurovector, Pavia, Italy). The pH-drift method was used to evaluate the pH_{PZC} of the sorbent.[66] Calcium chloride and sodium chloride solutions (0.1 and 1 M) were used as background salt. The pH of the background salt solutions was adjusted at different pH_0 values (in the range 2–11), before adding the sorbent (at sorbent dose: 2 g L^{-1}). The suspensions were maintained under shaking at 140 rpm and 20 ± 1 °C for 48 h. The final pH (pH_{eq}) was monitored using pH-meter (Inolab 7110 pH-meter, WTV, Munich, Germany). The equilibrium pH was plotted against pH_0; pH_{PZC} corresponds to the extrapolated value where $pH_{eq} = pH_0$.

Sorption and Desorption Tests: All the studies were performed in batch systems (agitation speed, v: 140 rpm) at 20 ± 1 °C and each experiment was performed in duplicate (average value and standard deviation are reported in the figures). A fixed amount of sorbent (*m*, g) was mixed with a volume of solution (*V*, L) containing a fixed amount of metal ion (C_0, mmol L^{-1}) at selected pH. For uptake kinetics, samples were collected at fixed time (*t*, min), filtrated (membrane filter: 1.2 µm) and analyzed for residual concentration ($C(t)$, mmol L^{-1}). For sorption isotherm, the contact time was fixed to 48 h. The pH was not controlled during the sorption tests but the final pH was systematically monitored. The concentration of the samples (C_0 and C_{eq}) was analyzed by an inductively coupled plasma atomic emission spectrometer ICP-AES ACTIVA M (Horiba Jobin Yvon, Longjumeau, France). The sorption capacity (i.e., q(t) or q_{eq}, mmol g^{-1}) was calculated using the mass balance equation:

$$q = \left(C_0 - C_{eq}\right) \times V/m \quad (4)$$

The same experimental procedure was applied for the investigation of sorption in bi-component solutions (equimolar solutions or variable molar ratio between the components), and for the sorption tests in presence of EDTA.

For the study of metal desorption and sorbent recycling, the batch method was also used. The sorbents were first preloaded with metal ion solutions (C_0: 1 mmol L^{-1}; sorbent dose, SD: 0.5 g L^{-1}; *v*: 140 rpm; t: 48 h). Two eluents HCl and 0.05 M $CaCl_2$ solutions at pH 2 were used for metal desorption by contact (under agitation for 24 h); using a SD of 0.5 g L^{-1}. After recovery of the eluted sorbents by filtration, the material was rinsed with deionized water and dried (at 50 °C for 12 h) before being re-used for a new sorption cycle. The concentration of the metal ions in the eluate was analyzed and the desorption efficiency (DE) was determined, at each cycle, by the mass balance equation and DE (%) = (Amount desorbed/Amount sorbed) × 100.

Note: Experimental conditions are systematically reported (briefly) in the caption of the Figures.

Metal Speciation and Sorption Modeling: The speciation of the metal ions under the different experimental conditions (for pH study, bi-component solutions and effect of EDTA) were calculated using Visual Minteq software.[67]

Modeling of uptake kinetics and sorption isotherms was performed using the conventional models summarized in Tables S2a and S2b, respectively. Pseudo-first and pseudo-second order rate equations,[40] and the Crank equation (for the resistance to intraparticle diffusion,[68]) were used for modeling kinetic profiles. The Langmuir, Freundlich, and Sips equations were used for fitting the sorption isotherms.[39] Model parameters were obtained using non-linear regression analysis and proprietary calculating notebook (through Mathematica facilities). The quality of the fits was analyzed using the determination coefficient (i.e., R^2) and the Akaike Information Criterion (AIC,[69] see Table S1, Supporting Information).

Supporting Information

Supporting Information is available from the Wiley Online Library or from the author.

Acknowledgements

This work was supported by the project PID 2021–126235OB-C32 of the Ministry of Science and Innovation (Spain), the projects UMA18-FEDERJA-126 and P20_00375 of Junta de Andalucía and FEDER funds. D.B.P. thanks the University of Málaga (Spain) for supporting post-doctoral contract. Y.Z. acknowledges the China Scholarship Council (CSC, Grant No. 201906660008) for Ph.D. fellowship. Authors thank Algaia SA for supplying AR.

Conflict of Interest

The authors declare no conflict of interest.

Data Availability Statement

The data that support the findings of this study are available from the corresponding author upon reasonable request.

Keywords

algal residues, enhanced separation of La(III) from base metals by selective EDTA complexation, sorbent recycling, sorption isotherm, sorption of heavy metals and lanthanum, uptake kinetics

[1] a) R. Shrestha, S. Ban, S. Devkota, S. Sharma, R. Joshi, A. P. Tiwari, H. Y. Kim, M. K. Joshi, *J. Environ. Chem. Eng.* **2021**, *9*, 105688; b) T. O. Ajiboye, O. A. Oyewo, D. C. Onwudiwe, *Chemosphere* **2021**, *262*, 128379.

[2] a) M. L. Sall, A. K. D. Diaw, D. Gningue-Sall, S. E. Aaron, J.-J. Aaron, *Environ. Sci. Pollut. Res.* **2020**, *27*, 29927; b) M. Zaynab, R. Al-Yahyai, A. Ameen, Y. Sharif, L. Ali, M. Fatima, K. A. Khan, S. Li, *J. King Saud Univ. Sci.* **2022**, *34*, 101653.

[3] a) Y. Cao, P. Shao, Y. Chen, X. Zhou, L. Yang, H. Shi, K. Yu, X. Luo, X. Luo, *Resour. Conserv. Recycl.* **2021**, *169*, 105519; b) T. G. Ambaye, M. Vaccari, F. D. Castro, S. Prasad, S. Rtimi, *Environ. Sci. Pollut. Res.* **2020**, *27*, 36052.

[4] a) L. Tofan, C.-N. Bojoaga, C. Paduraru, *Environ. Chem. Lett.* **2022**, *20*, 1225; b) A. T. Nakhjiri, H. Sanaeepur, A. E. Amooghin, M. M. A. Shirazi, *Desalination* **2022**, *527*, 115510.

[5] A. Hartwig, in *Cadmium: From Toxicity to Essentiality* (Eds.: A. Sigel, H. Sigel, R. K. O. Sigel), Springer, Dordrecht **2013**, pp. 491–507.

[6] F. Xie, T. A. Zhang, D. Dreisinger, F. Doyle, *Miner. Eng.* **2014**, *56*, 10.

[7] N. A. Mancheri, B. Sprecher, G. Bailey, J. Ge, A. Tukker, *Resour. Conserv. Recycl.* **2019**, *142*, 101.

[8] a) W. C. M. de Oliveira, G. D. Rodrigues, A. B. Mageste, L. R. de Lemos, *Chem. Eng. J.* **2017**, *322*, 346; b) V. Agarwal, M. K. Khalid, A. Porvali, B. P. Wilson, M. Lundström, *Sustainable Mater. Technol.* **2019**, *22*, e00121.

[9] a) E. O. Opare, E. Struhs, A. Mirkouei, *Renewable Sustainable Energy Rev.* **2021**, *143*, 110917; b) L. Omodara, S. Pitkaaho, E.-M. Turpeinen, P. Saavalainen, K. Oravisjarvi, R. L. Keiski, *J. Cleaner Prod.* **2019**, *236*, 117573.

[10] a) W. S. Chai, J. Y. Cheun, P. S. Kumar, M. Mubashir, Z. Majeed, F. Banat, S.-H. Ho, P. L. Show, *J. Cleaner Prod.* **2021**, *296*, 126589; b) A. Azimi, A. Azari, M. Rezakazemi, M. Ansarpour, *ChemBioEng Rev.* **2017**, *4*, 37.

[11] L. Castro, M. L. Blazquez, F. Gonzalez, J. A. Munoz, A. Ballester, *Sci. Total Environ.* **2017**, *598*, 856.

[12] M. M. Montazer-Rahmati, P. Rabbani, A. Abdolali, A. R. Keshtkar, *J. Hazardous Mater.* **2011**, *185*, 401.

[13] a) M. Priyadarshanee, S. Das, *J. Environ. Chem. Eng.* **2021**, *9*, 104686; b) E. H. FodayJr, B. Bo, X. Xu, *Sustainability* **2021**, *13*, 12311.

[14] a) P. R. Yaashikaa, P. S. Kumar, A. Saravanan, D.-V. N. Vo, *J. Hazardous Mater.* **2021**, *420*, 126596; b) H. I. Syeda, I. Sultan, K. S. Razavi, P.-S. Yap, *J. Water Process Eng.* **2022**, *46*, 102446; c) H. Qin, T. Hu, Y. Zhai, N. Lu, J. Aliyeva, *Environ. Poll.* **2020**, *258*, 113777; d) A. Agarwal, U. Upadhyay, I. Sreedhar, S. A. Singh, C. M. Patel, *J. Water Process Eng.* **2020**, *38*, 101602; e) S. Gavriely, S. Richter, I. Zucker, *Adv. Sustainable Syst.* **2022**, *6*, 2200081.

[15] a) S. Mathew, J. C. Soans, R. Rachitha, M. S. Shilpalekha, S. G. S. Gowda, P. Juvvi, A. K. Chakka, *J. Food Sci. Technol.* **2022**. https://doi.org/10.1007/s13197-022-05486-1. b) A. M. Elgarahy, K. Z. Elwakeel, S. H. Mohammad, G. A. Elshoubaky, *Cleaner Eng. Technol.* **2021**, *4*, 100209.

[16] S. Rajendran, A. K. Priya, P. S. Kumar, T. K. A. Hoang, K. Sekar, K. Y. Chong, K. S. Khoo, H. S. Ng, P. L. Show, *Chemosphere* **2022**, *303*, 135146.

[17] a) A. T. Ubando, A. D. M. Africa, M. C. Maniquiz-Redillas, A. B. Culaba, W.-H. Chen, J.-S. Chang, *J. Hazardous Mater.* **2021**, *402*, 123431; b) Z. A. Sutirman, M. M. Sanagi, W. I. W. Aini, *Int. J. Biol. Macromol.* **2021**, *174*, 216; c) T. Du, A. Bogush, O. Masek, S. Purton, L. C. Campos, *Chemosphere* **2022**, *304*, 135284.

[18] a) M. E. Romero-González, C. J. Williams, P. H. E. Gardiner, *Environ. Sci. Technol.* **2001**, *35*, 3025; b) N. A. Negm, M. G. Abd El Wahed, A. R. A. Hassan, M. T. H. Abou Kana, *J. Mol. Liq.* **2018**, *264*, 292.

[19] F. Almomani, R. R. Bhosale, *Sci. Total Environ.* **2021**, *755*, 142654.

[20] N. Ahalya, T. V. Ramachandra, R. D. Kanamadi, *Res. J. Chem. Environ.* **2003**, *7*, 71.

[21] a) R. Li, T. Zhang, H. Zhong, W. Song, Y. Zhou, X. Yin, *Environ. Technol.* **2021**, *42*, 3132; b) S. Y. Cheng, P. L. Show, B. F. Lau, J. S. Chang, T. C. Ling, *Trends Biotechnol.* **2019**, *37*, 1255.

[22] S. K. Mehta, J. P. Gaur, *Crit. Rev. Biotechnol.* **2005**, *25*, 113.

[23] N. Kuyucak, B. Volesky, *Biotechnol. Bioeng.* **1989**, *33*, 823.

[24] A. Singh, P. S. Nigam, J. D. Murphy, *Bioresour. Technol.* **2011**, *102*, 10.

[25] a) R. V. Kapoore, E. E. Wood, C. A. Llewellyn, *Biotechnol. Adv.* **2021**, *49*, 107754; b) S. Han, J. S. Park, S. Umanzor, C. Yarish, J. K. Kim, *Sci. Rep.* **2022**, *12*, 11878.

[26] M. Fomina, G. M. Gadd, *Bioresour. Technol.* **2014**, *160*, 3.

[27] J. M. Lezcano, F. Gonzalez, A. Ballester, M. L. Blazquez, J. A. Munoz, C. Garcia-Balboa, *Chem. Ecol.* **2010**, *26*, 1.

[28] D. Bulgariu, L. Bulgariu, *Bioresour. Technol.* **2012**, *103*, 489.

[29] D. Bulgariu, L. Bulgariu, *J. Cleaner Prod.* **2016**, *112*, 4525.

[30] H. Saleem, U. Rafique, R. P. Davies, *Microporous Mesoporous Mater.* **2016**, *221*, 238.

[31] Y. Ibrahim, A. Kassab, K. Eid, A. M. Abdullah, K. I. Ozoemena, A. Elzatahry, *Nanomaterials* **2020**, *10*, 885.

[32] a) B. Kloareg, R. S. Quatrano, *Oceanogr. Mar. Biol.* **1988**, *26*, 259; b) D. Manns, M. Nielsen, A. Bruhn, B. Saake, A. Meyer, *J. Appl. Phycol.* **2017**, *29*, 1493; c) M. Fertah, A. Belfkira, E. m. Dahmane, M. Taourirte, F. Brouillette, *Arabian J. Chem.* **2017**, *10*, S3707.

[33] S. K. Papageorgiou, E. P. Kouvelos, E. P. Favvas, A. A. Sapalidis, G. E. Romanos, F. K. Katsaros, *Carbohydr. Res.* **2010**, *345*, 469.

[34] M. A. Fawzy, M. Gomaa, A. F. Hifney, K. M. Abdel-Gawad, *Carbohydr. Polym.* **2017**, *157*, 1903.

[35] P. Shao, D. Liang, L. Yang, H. Shi, Z. Xiong, L. Ding, X. Yin, K. Zhang, X. Luo, *J. Hazardous Mater.* **2020**, *387*, 121676.

[36] F. Wei, H. Tu, Y. Wang, S. Yue, J. Du, *J. Phys. Conf. Ser.* **2009**, *152*, 012003.

[37] Q.-Q. Liu, K.-F. Yue, X.-J. Weng, Y.-Y. Wang, *CrystEngComm* **2019**, *21*, 6186.

[38] A. Naskar, A. K. Guha, M. Mukherjee, L. Ray, *Sep. Sci. Technol.* **2016**, *51*, 427.

[39] C. Tien, *Adsorption Calculations and Modeling*, Butterworth-Heinemann, Boston **1994**.

[40] Y. S. Ho, G. McKay, *Process Biochem.* **1999**, *34*, 451.

[41] S. A. Allahyari, R. Saberi, K. Sepanloo, A. Lashkari, *J. Rare Earths* **2021**, *39*, 742.

[42] V. R. Moreira, Y. A. R. Lebron, L. C. Lange, L. V. S. Santos, *J. Environ. Manage.* **2019**, *251*, 109587.

[43] Y. Marcus, *Ion Properties*, Marcel Dekker, Inc. , New York **1997**.

[44] J. Buffle, Z. Zhang, K. Startchev, *Environ. Sci. Technol.* **2007**, *41*, 7609.

[45] E. Karnio, Y. Fujiwara, M. M. Urnoto, F. Valenzuela, K. Kondo, *Chem. Eng. J.* **2008**, *139*, 93.

[46] D. Kolodynska, D. Fila, Z. Hubicki, *Environ. Res.* **2020**, *191*, 110171.

[47] S. K. Papageorgiou, E. P. Kouvelos, F. K. Katsaros, *Desalination* **2008**, *224*, 293.

[48] R. G. Pearson, *Science* **1966**, *151*, 172.

[49] E. Romera, F. González, A. Ballester, M. L. Blázquez, J. A. Muñoz, *Bioresour. Technol.* **2007**, *98*, 3344.

[50] K. Vijayaraghavan, M. Sathishkumar, R. Balasubramanian, *Ind. Eng. Chem. Res.* **2010**, *49*, 4405.

[51] J. R. Guarín-Romero, P. Rodríguez-Estupiñán, L. Giraldo, J. C. Moreno-Piraján, *ACS Omega* **2019**, *4*, 18147.

[52] J. Long, X. Huang, X. Fan, Y. Peng, J. Xia, *Water Sci. Technol.* **2018**, *78*, 156.

[53] M. Kumar, A. K. Singh, M. Sikandar, *Appl. Water Sci.* **2018**, *8*, 225.

[54] M. Plöhn, C. Escudero-Oñate, C. Funk, *Algal Res.* **2021**, *59*, 102471.

[55] M. C. Palmieri, B. Volesky, O. Garcia, *Hydrometallurgy* **2002**, *67*, 31.

[56] Z. S. Birungi, E. Chirwa, *Chem. Eng. Trans.* **2018**, *64*, 535.

[57] S. K. Kazy, S. K. Das, P. Sar, *J. Ind. Microbiol. Biotechnol.* **2006**, *33*, 773.

[58] T. B. da Costa, M. G. C. da Silva, M. G. A. Vieira, *J. Hazard. Mater.* **2022**, *421*, 126742.

[59] D. Wu, J. Zhao, L. Zhang, Q. Wu, Y. Yang, *Hydrometallurgy* **2010**, *101*, 76.
[60] C. Menakbi, F. Quignard, T. Mineva, *J. Phys. Chem. B* **2016**, *120*, 3615.
[61] Y. Chen, X. G. Ma, J. B. Peng, *Carbohydr. Polym.* **2021**, *271*, 118435.
[62] E. R. Engel, V. Calabrese, K. M. Z. Hossain, K. J. Edler, J. L. Scott, *Adv. Sustainable Syst.* **2021**, *5*, 2000069.
[63] Y. Zhang, M. F. Hamza, T. Vincent, J.-C. Roux, C. Faur, E. Guibal, *Chem. Eng. J.* **2021**, *431*, 133214.
[64] Y. G. Wang, Y. Xiong, S. L. Meng, D. Q. Li, *Talanta* **2004**, *63*, 239.
[65] a) A. A. Galhoum, E. A. Elshehy, D. A. Tolan, A. M. El-Nahas, T. Taketsugu, K. Nishikiori, T. Akashi, A. S. Morshedy, E. Guibal, *Chem. Eng. J.* **2019**, *375*, 121932; b) M. F. Hamza, Y. Wei, H. I. Mira, A. A. H. Abdel-Rahman, E. Guibal, *Chem. Eng. J.* **2019**, *362*, 310; c) M. F. Hamza, Y. Wei, A. Benettayeb, X. Wang, E. Guibal, *J. Mater. Sci.* **2020**, *55*, 4193.
[66] M. V. Lopez-Ramon, F. Stoeckli, C. Moreno-Castilla, F. Carrasco-Marin, *Carbon* **1999**, *37*, 1215.
[67] J. P. Gustafsson, Visual MINTEQ, https://vminteq.lwr.kth.se/, 2013, Vers. 3.1, KTH, Royal Institute of Technology, Stockholm, Sweden, (accessed: April 2019).
[68] J. Crank, *The Mathematics of Diffusion*, 2nd. ed., Clarendon Press, Oxford **1975**.
[69] O. Falyouna, O. Eljamal, I. Maamoun, A. Tahara, Y. Sugihara, *J. Colloid Interface Sci.* **2020**, *571*, 66.